Open access • Journal Article • DOI:10.1103/PHYSREVA.53.3358

# Bichromatic atomic lens. — Source link

M. K. Olsen, T. Wong, S. M. Tan, D. F. Walls

**Published on:** 01 May 1996 - Physical Review A (American Physical Society)

**Topics:** Optical field, Light field, Field (physics), Thin lens and Standing wave

# Bichromatic atomic lens

M. K. Olsen, T. Wong, S. M. Tan, and D. F. Walls
*Department of Physics, University of Auckland, Private Bag 92019, Auckland, New Zealand*
(Received 5 September 1995)

We investigate the focusing of three-level atoms with a bichromatic standing wave laser field, using both classical and quantum treatments of the problem. We find that, for the appropriate ratio of detunings to Rabi frequencies, the atoms will experience a periodic potential which is close to harmonic across half an optical wavelength. The field thus becomes equivalent to a periodic array of microlenses, which could be utilized to deposit lines of atoms upon a substrate. We consider and compare two regimes, differentiated by the interaction time of the atoms in the optical field. The first case considered, the Raman-Nath regime, is analogous to the thin lens regime in classical optics. The second case treats the transverse atomic motion within the light field, and investigates the distribution of atoms upon a substrate placed within the field. We investigate the extent to which this case can be modeled classically.

PACS number(s): 03.75.Be, 42.50.Vk, 03.65.Sq

## I. INTRODUCTION

The mechanical manipulation of atoms by light is a field of active interest, including such processes as laser cooling, atom trapping, atomic focusing, and beam splitting [1,2]. Although the scattering of electrons by light was predicted as early as 1933 [3], it was not until 1966 that this optical scattering effect was predicted for neutral atoms [4], becoming known as the Kapitza-Dirac effect. The first experimental realization of optical diffraction of atoms in which the experimental conditions were sufficiently well defined to permit a clear-cut comparison with theory was reported by Gould, Ruff, and Pritchard in 1986 [5]. The observed results were found to be in good agreement with theoretical predictions.

Letokhov predicted in 1968 that atoms within an optical standing wave could be either attracted or repelled by the antinodes of the field, changing their velocity distribution [6], while Kazantsev and collaborators [7] predicted the presence of velocity-dependent forces acting upon atoms moving in an intense standing wave. The successful confinement of neutral atoms in optical wavelength size regions between the peaks of an optical standing wave, known as channeling, was reported by Salomon *et al.* in 1987 [8]. The forces on stationary $\Lambda$ configuration atoms in arbitrary combinations of two standing and traveling wave fields were calculated by Prentiss *et al.* [9]. Using a zero-velocity approximation with the optical Bloch equations, they showed that the force on the atom can have components varying on a scale much less than the optical wavelength, the scale being controlled by varying the relative phase of the two optical fields. A recent study of the near field regime of diffractive atom optics by Janicke and Wilkens [10] investigates the focusing of wave packets using two-level optical systems. They conclude that the technique has potential applications for atom lithography.

The localization of rubidium atoms in the ladder configuration has recently been observed by Grove *et al.* [11]. The rectified dipole force resulting from an intense bichromatic standing wave produces localization of cold atoms in potential wells with a period of 71 $\mu$m. This experiment, in which subwavelength channeling was not present, relies on two-photon resonance with the ladder atom to completely rectify the force on the wavelength scale.

Recent experiments by McClelland *et al.* [12] and Gupta *et al.* [13] have used monochromatic laser focusing in both one and two dimensions to deposit chromium atoms on a silicon substrate. In one dimension, the authors used atom force microscopy to measure a linewidth of $65\pm6$ nm for the deposited lines of atoms, corresponding to $0.15\lambda_L$, but were not able to accurately predict their results using a semiclassical model. In two dimensions, features $13\pm1$ nm high, with a full width at half maximum (FWHM) of $80\pm10$ nm, were fabricated in a square array with a lattice constant of 212.78 nm, or half the laser wavelength. The array covered an area of approximately $100\times200$ $\mu$m. Blockley [14] has undertaken a theoretical investigation which, applying a quantum treatment, manages to produce most of the features of the one-dimensional experiment of McClelland *et al.*

## II. MOTIVATION

It is well known from classical mechanics that particles placed at various positions in a parabolic well will all reach the bottom after the same time interval. In classical optics a parabola is known as one of the Cartesian surfaces which will form perfect images by reflection or refraction. Making the comparison between atom optics and classical physics, we might expect that the ideal mechanism for laser focusing would utilize an optical potential with a parabolic spatial dependence. One of the eigenpotentials derived from the diagonalization of the interaction Hamiltonian of a two-level atom with a standing wave field exhibits a shape which is close to quadratic across part of a period. The anharmonicity resulting from the nonquadratic portion of the potential means that it will be difficult to obtain sharp atomic focusing using the two-level mechanism.

In a previous work [15], which investigated the utility of bichromatic standing wave laser fields as a beam splitter for three-level atoms, the present authors found that one of the eigenpotentials of the interaction Hamiltonian has a form which, for certain combinations of Rabi frequencies and detunings, is very close to quadratic. A potential with the same

 

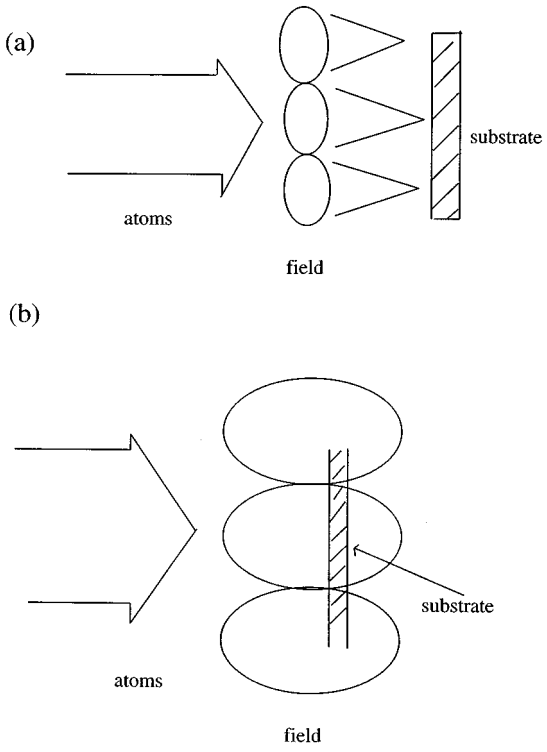


FIG. 1. Simplified schematic of the systems of atoms and fields for the bichromatic atomic lens. The thin lens system is illustrated by (a), while (b) demonstrates the configuration required for channeling.

shape can also be created using a combination of optical and magnetic fields [16], but magnetic fields are not always desirable in practical applications. The present work is an investigation of the usefulness of the bichromatic potential for the focusing of atomic beams, in which we both investigate the need for a full quantum description and compare the expected performance with that theoretically available from a two-level system. Although the following analysis is specifically for atoms in the ladder configuration, the performance of the system with $\Lambda$ or $V$ atoms is almost identical until spontaneous emission is considered. As we shall demonstrate below, spontaneous emission is not expected to be the main cause of performance degradation, so that there is some degree of experimental freedom in the choice of atom.

## III. THE SYSTEMS

There are two different mechanisms for achieving focusing using our system, as schematically illustrated in Fig. 1. Depending on whether the atoms are deposited outside of, or within the standing wave field, we describe these mechanisms as *thin lensing* and *channeling,* respectively. The first situation, analogous to the thin lens regime in classical optics, treats the atom-field interaction using the Raman-Nath approximation. The substrate on which we wish to place lines of atoms is positioned outside the field, in a position analogous to the focal plane of an optical lens. The second situation, applicable for longer interaction times, investigates atomic motion within the field. This situation can be compared to the classical problem of point masses in a potential

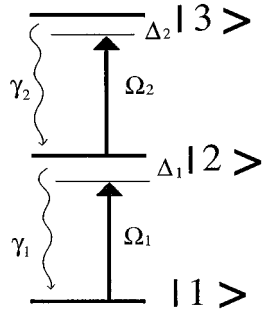


FIG. 2. Configuration of a generic three-level ladder atom. The Rabi frequencies imposed on each transition by laser fields with frequency $\omega_j$ are represented by $\Omega_j$, the detunings by $\Delta_j$, and the spontaneous emission rates by $\gamma_j$, for all of which $j=1,2$.

well. In this, the regime of the experiments of McClelland and co-workers [12,13], the substrate is placed at some position within the laser fields.

Our analysis is two dimensional, with the atomic beam traveling in the $x$ direction and the two standing waves being formed in the $z$ direction. We have investigated the performance of this scheme for three-level atoms in the ladder configuration, although most of the analysis would also apply to atoms in the $\Lambda$ and $V$ configurations. The coherent evolutions for these three atomic configurations, as long as we consider only single-photon transitions, are exactly the same. Differences arise once we consider spontaneous emission, but, as we shall demonstrate below, this will have a negligible effect on performance compared with other expected defocusing mechanisms.

The atomic configuration of a ladder atom is as shown in Fig. 2. The frequencies of the laser fields applied to the atoms are represented by $\omega_j$, the detuning of these fields from resonance by $\Delta_j$, the effective Rabi frequencies by $\Omega_j$, and the respective spontaneous emission rates by $\gamma_j$, in all of which $j=1,2$. In contrast to the experiment of Grove *et al.*, [11] our system is not two-photon resonant, as we are not seeking to rectify the dipole force on the wavelength scale. The polarization of each standing wave field is chosen so that it can only drive one transition. The combined system of atom and fields can be represented in Dirac notation using the basis states $|1,m+1,n\rangle$, $|2,m,n\rangle$, and $|3,m,n-1\rangle$, where the first number represents the atomic energy level, $m$ represents the number of photons in the laser field with frequency $\omega_1$, and $n$ refers to $\omega_2$. We assume that $m$ and $n$ are large enough so that $m\approx m-1$ and $n\approx n-1$. We will refer to these states via the shorthand notation $|1\rangle$, $|2\rangle$, and $|3\rangle$.

The system Hamiltonian is developed within the rotating wave and electric dipole approximations. Using $a$ and $a^\dagger$ as the boson operators for the laser field associated with $\omega_1$, and $b$ and $b^\dagger$ for $\omega_2$, we can write the Hamiltonian as

$$\mathcal{H}=\mathcal{H}_f+\mathcal{H}_a+\mathcal{H}_{\rm int}+\mathcal{H}_{\rm kin}, \tag{1}$$

where the Hamiltonian for the free fields is

$$\mathcal{H}_f=\hbar(\omega_1 a^\dagger a+\omega_2 b^\dagger b). \tag{2}$$

The atomic Hamiltonian is

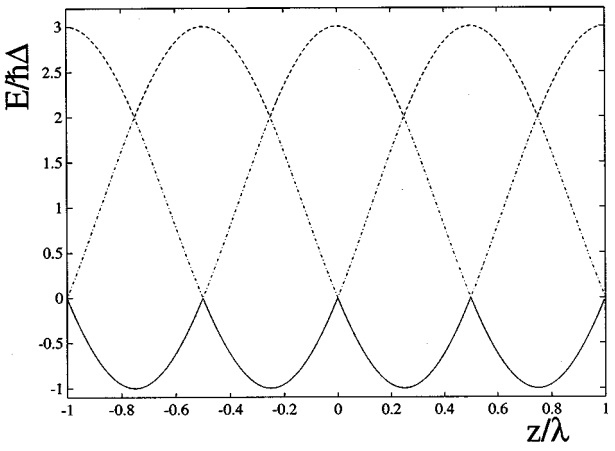


FIG. 3. Eigenpotentials of $\mathscr{V}$ for $\Omega_1=\Omega_2=2\sqrt{2}\Delta$. The energies are scaled such that $\hbar=k=\Delta=1$.

$$\mathscr{H}_a=\hbar\{(\omega_1+\Delta_1)\sigma_{22}+(\omega_1+\omega_2+\Delta_1+\Delta_2)\sigma_{33}\}, \quad (3)$$

the interaction Hamiltonian is

$$\mathscr{H}_{\rm int}=\frac{\hbar}{2}\{(g_1 a\sigma_{21}+g_1^* a^\dagger\sigma_{12})\sin kz+(g_2 b\sigma_{32} +g_2^* b^\dagger\sigma_{23})\sin(kz+\phi)\}, \quad (4)$$

and the kinetic term is

$$\mathscr{H}_{\rm kin}=\vec{p}\cdot\vec{p}/2m. \quad (5)$$

In the above equations, the $\sigma_{ij}$ are the atomic population and coherence operators, $g_j$ are the coupling constants for the appropriate fields and transitions, $\phi$ is the phase difference between the two standing waves, $k$ can be taken as the average wave number for the two fields, and $\vec{p}$ and $m$ are the atomic momentum and mass, respectively. A condition which must be satisfied here is that $k\approx k_1\approx k_2$ so that the correct phase relationship is preserved across the interaction region. This would put experimental constraints on the choice of atoms.

We can now develop an effective semiclassical Hamiltonian,

$$\mathbf{H}_{\rm sc}=\mathscr{H}_{\rm kin}+\mathscr{V}. \quad (6)$$

The effective interaction term $\mathscr{V}$, after discarding a constant diagonal term, can be written in matrix form as

$$\mathscr{V}=\frac{\hbar}{2}\begin{bmatrix} 0 & \Omega_1\sin kz & 0 \\ \Omega_1^*\sin kz & 2\Delta_1 & \Omega_2\sin(kz+\phi) \\ 0 & \Omega_2^*\sin(kz+\phi) & 2(\Delta_1+\Delta_2) \end{bmatrix}, \quad (7)$$

in which $g_1 a$ and $g_2 b$ have been changed to their respective semiclassical equivalents, $\Omega_1$ and $\Omega_2$. The basis vectors are $|1\rangle$, $|2\rangle$, and $|3\rangle$ as defined above.

Since we are investigating a three-level system, we find that the Hamiltonian has three eigenpotentials, corresponding to three different atomic eigenstates. For the correct choice of Rabi frequencies and detunings, we find that the three potentials come together via avoided crossings at certain points and the bottom potential can be seen to approximate a series of harmonic oscillators, see Fig. 3. The Rabi frequencies and detunings chosen, $\Delta_1=\Delta_2=\Delta$, with $\Omega_j=2\sqrt{2}\Delta$ $(j=1,2)$, are the same as used for the ladder system in the authors' earlier analysis of the bichromatic beam splitter [15]. We have investigated the effect of differing ratios of Rabi frequency to detuning on the harmonicity of the potential and find the optimal ratio to be close to $\Omega_j/\Delta=2\sqrt{2}$. This can be seen by examination of Fig. 4(b), in which least squares measures of deviation from the exactly harmonic are plotted against the ratio $\Omega_j/\Delta$. Although there is a definite minimum in both the curves, the performance of the bichromatic atomic lens is not as sensitive to the exact ratio $\Omega_j/\Delta$ as is the bichromatic beam splitter. We found in numerical simulations that the system has good focusing properties over at least the range $\sqrt{3}\leq\Omega_j/\Delta\leq 2\sqrt{3}$.

Only those atoms in the appropriate eigenstate will experience the desired quadratic potential. As the Rabi frequencies go to zero, this eigenstate tends to become $|1\rangle$, the ground state of the ladder atom. We can therefore take ad-

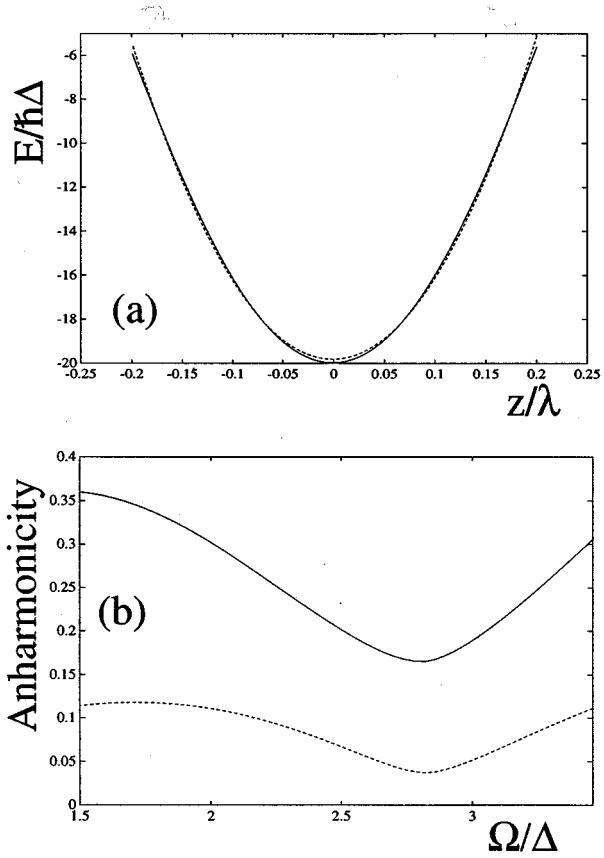


FIG. 4. (a) Atomic phase shift as a function of position, derived from integrating the bottom potential across the profile of the bichromatic standing wave. The optical parameters are as in Fig. 3. The dashed curve is a quadratic approximation to the phase shift. (b) Least squares measures of the deviation from ideal harmonicity of the potential as functions of the ratio $\Omega_j/\Delta$. Plotted in arbitrary units, the solid line defines the ideal quadratic using the second derivative at the origin, while the dashed line uses a polynomial fitting package.

vantage of the fact that, if the atoms are not traveling too fast, those that enter the field in $|1\rangle$ will tend to adiabatically follow the potential as it varies over the Gaussian profile of a real standing wave. Our numerical simulations of the transit of atoms across a Gaussian profile field demonstrate that a high degree of adiabaticity ($>90\%$) can be expected. The Gaussian profile of real standing waves also means that the atoms will only experience the appropriate quadratic potential over a portion of their transit time. By comparison with theoretical fields with a *top hat* profile, this will also tend to decrease the harmonicity of the accumulated phase shift.

We have used a modification of the rms width to characterize the narrowness of the atomic distributions so that we can quantitatively compare our results with those expected from a two-level system, as well as quantifying the effects of the broadening mechanisms we will investigate. Although the FWHM measure gives little weight to any small background which may be present, we felt that the standard rms measure would tend to give too much weight to the wings of a distribution. For a distribution extending over half a wavelength, our measure of width is defined as

$$\mathscr{W}_c=\left[\frac{\int_0^{\pi}\cos^2 z|\psi(z)|^2dz}{\int_0^{\pi}|\psi(z)|^2dz}\right]^{1/2}, \tag{8}$$

noting that $\pi$ corresponds to $\lambda_L/2$ since we have set $k=1$.

## IV. THIN LENS REGIME

In the thin lens, Raman-Nath regime, we ignore transverse atomic motion within the field. Formally, this imposes a condition on the interaction time,

$$t<t_{\mathrm{RN}}=(\omega_R\Omega_j)^{-1/2}, \tag{9}$$

where $\omega_R=\hbar k^2/2m$, with $m$ as the atomic mass, is the recoil frequency and $\Omega_j$ is the larger of the two Rabi frequencies. In practice there will always be some transverse atomic motion within the field, with the Raman-Nath approximation being valid when this is a negligible fraction of the optical wavelength.

Within this approximation, the effect of the field is to cause a phase shift across the atomic wave front, so that the atomic wave function after the field attains a position-dependent transverse momentum distribution. Analogously to geometric optics, the wave function will become focused some distance beyond the field, allowing lines of atoms to be deposited on a substrate placed at the appropriate location.

The effective position-dependent Hamiltonian, Eq. (7), is used to calculate the time development of the atomic wave function in the position representation as it crosses the standing wave field with transit time $t$. Since $[\mathscr{V}(t),\mathscr{V}(t')]=0\ \forall t,t'$, we can write

$$\Psi(z,t)=\Psi(z,0)\exp\left[\frac{-i}{\hbar}\int_0^t\mathscr{V}dt\right], \tag{10}$$

from which the momentum probability distribution after transitting the field is obtained via Fourier transform,

$$\Phi(p,t)=\mathscr{F}[\Psi(z,t)]. \tag{11}$$

The kinetic operator $\mathbf{H}_{\mathrm{kin}}$ is then used to propagate $\Phi(p,t)$ through free space, for time $t_f$, to the substrate,

$$\Phi(p,t+t_f)=\Phi(p,t)\exp\left[\frac{-i}{\hbar}\int_t^{t+t_f}\mathbf{H}_{\mathrm{kin}}dt\right], \tag{12}$$

which enables calculation of the position wave function at the focus, via inverse Fourier transform,

$$\Psi(z,t+t_f)=\mathscr{F}^{-1}[\Phi(p,t+t_f)]. \tag{13}$$

The atomic spatial distribution at the focus is then found by taking the absolute square of the position wave function, $|\Psi(z,t+t_f)|^2$.

An approximate analytical expression can be readily calculated for the focal length of a two-level atomic lens using the methods of classical optics. Janicke and Wilkens [10], for example, have performed these calculations, deriving expressions for the focal length and the focal spot size in the two-level case. For the three-level system, however, an analytical expression which is valid for arbitrary parameters is not easily derived. We have restricted ourselves to numerical calculations valid for each choice of Rabi frequency, wavelength, atomic mass and detuning.

The classical optical formula for the phase shift across a plane wave impinging on a section of lens,

$$\delta\phi=kz^2/2f, \tag{14}$$

can also be used to find the focal length for our bichromatic atomic lens. In our case the phase shift is the integral of the appropriate eigenpotential across the laser field and the de Broglie wave number $k_{\mathrm{dB}}$ is substituted for the optical wave number,

$$k_{\mathrm{dB}}z^2/2f=\int_0^t\mathscr{U}(z,t)dt/\hbar, \tag{15}$$

where $\mathscr{U}(z,t)$ is the desired quadratic potential. We find that the potential, even when integrated over the Gaussian profile of a laser field, still gives a phase shift which has a closely quadratic position dependence, as shown in Fig. 4(a).

Use of a least squares polynomial fitting routine allows us to approximate the phase shift across half a wavelength by a quadratic in $z$,

$$\int_0^t\mathscr{U}(z,t)dt/\hbar\approx\mathscr{C}(z-z_0)^2+V_0, \tag{16}$$

where $z_0$ is the position of minimum phase shift, $V_0$. Using Eqs. (15) and (16) and remembering that $\hbar=1$ in our system of units, we can derive an expression for the flight time of an atom to the focal plane,

$$t_f=m/2\mathscr{C}. \tag{17}$$

We found that, by fitting the phase shift curve only between the two points of inflection, we were able to estimate the focal length to within $\approx 5\%$ of the empirically determined value, demonstrating that anharmonicity does not play a major role in this system.

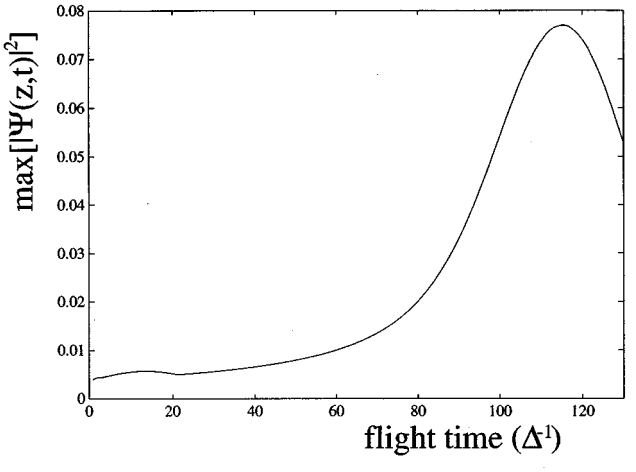


FIG. 5. Maximum of $|\psi(z,t)|^2$ as a function of flight time after the field, for the thin lens system.

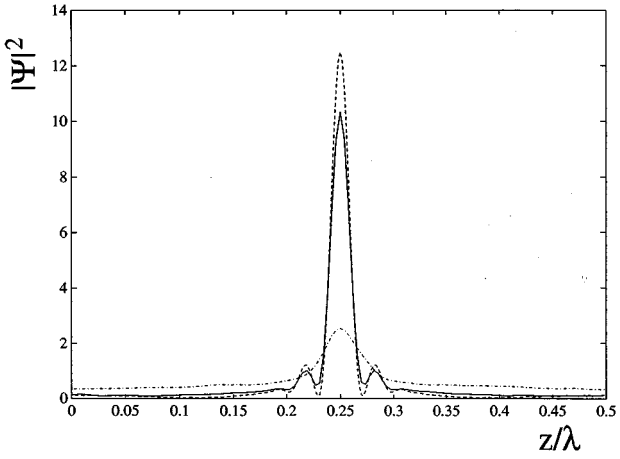


FIG. 6. Atomic distributions at the focus of the thin lens system, for the optical parameters described in the text and a flight time of $115|\Delta|^{-1}$. Note that all atomic distribution plots are normalized so that $\int_0^{\lambda/2}|\psi|^2dz=1$. The dashed line results from considering the coherent evolution only. The solid line includes spontaneous emission effects with decay rates of $\gamma_1=\gamma_2=\Omega/100$. The bottom, dash-dotted line is the result for $\gamma_1=\gamma_2=\Omega/10$.

We have used a somewhat arbitrary atomic mass of 2000 for our numerical simulations in the thin lens regime, which allows us to calculate $t_f$ in units of $\Delta^{-1}$. Remembering that $\hbar=k=1$, this means $t_{\mathrm{RN}}\approx 38/\Delta$. The atomic wave packet is treated as a plane wave, while the laser field is given a Gaussian profile. In the frame which follows the longitudinal motion of the atom across the light field, the Gaussian amplitude variation of the standing wave field gives rise to an effective temporal variation. This variation is also of Gaussian form and has a standard deviation of $12/\sqrt{2}|\Delta|$, with the field extending over $\pm 4.25$ standard deviations. The value of $12|\Delta|^{-1}$ corresponds closely to the atomic crossing time over the $1/e$ intensity half-width which is often used to characterize a laser beam experimentally. The Rabi frequencies at the peak of the Gaussian are set at 1.1 times the optimal value in an attempt to have the atoms experience the desired potential for a worthwhile time interval.

The flight time from the field to the focal plane is found from the numerical results by calculating the maximum of $|\psi(z,t)|^2$ at each time step. This will have its maximum value when the atomic distribution is most sharply focused, as shown in Fig. 5. The atomic distribution at the focus resulting from a calculation using the above parameters is shown in Fig. 6, demonstrating that the plane wave becomes sharply focused, with little in the way of background. The near harmonicity of the potential is demonstrated by the fact that the predicted focal time is $109|\Delta|^{-1}$, whereas the empirically determined time is $115|\Delta|^{-1}$. The atomic distributions at these two times are almost indistinguishable when plotted on the scale of Fig. 6. Using the formula of Eq. (8), the peak width for this somewhat idealized situation of an atomic plane wave with zero initial transverse velocity is found to equal $0.043\lambda_L$. This demonstrates that the bichromatic atomic lens is capable, in principle, of producing linewidths of very much less than an optical wavelength. The FWHM measure for this distribution is $0.012\lambda_L$. We realize that these widths will not be achievable in practice, but to give some idea of what is actually achievable we will investigate some of the possible broadening mechanisms below, in Sec. VI.

## V. CHANNELING WITHIN THE LASER FIELDS

The thin lens, Raman-Nath, approximation is only applicable to the cases where the interaction time between the atoms and the field is such that the transverse kinetic energy gained by the atoms remains much less than the depth of the light-induced potential. In physical terms, this means that we ignore any transverse atomic motion within the field. In reality, the atoms will develop a transverse momentum component which, in the bichromatic system under investigation, means that they will oscillate within the potential, focusing and defocusing with a period dependent on the square root of the atomic mass. This motion within the field, known as *channeling*, was first observed experimentally by Salomon *et al.* [8] and is the mechanism used for focusing chromium atoms in the experiment of McClelland and co-workers [12,13]. While the single standing wave potentials used for channeling in the above experiments can only be considered as near harmonic over a small portion of their wavelengths, the bichromatic potential is closely harmonic over most of a half-wavelength period, promising much better performance for atom lithography.

The physical apparatus required to focus atoms by the channeling mechanism differs from the thin lens apparatus in that the substrate now needs to be placed within the laser field, as in Fig. 1(b). The optimum position for the substrate can be closely calculated by considering the period of a harmonic oscillator. Writing the harmonic oscillator potential as

$$y=\tfrac{1}{2}m\omega^2z^2, \tag{18}$$

where $m$ is a particle mass and $\omega$ is the oscillation frequency, the period $T$ is simply $2\pi/\omega$. As in Sec. IV, we can fit our calculated potential with a quadratic, Eq. (16), so that the period of oscillation becomes

$$T=\pi\sqrt{2m/\mathscr{C}}. \tag{19}$$

The small degree of anharmonicity of the bichromatic potential means that the first focal plane will give the narrowest distribution, with subsequent peaks broadening as individual atoms tend to be refocused after different times. The first focal plane for a plane wave input beam is found after a flight time $t_c \approx T/4$.

The atomic motion within the field cannot be calculated by direct time integration of the Hamiltonian as in Eq. (10), since the two terms in the full Hamiltonian, Eq. (6), do not commute. We have therefore used an incremental symmetrized split-operator method [17], accurate to third order in the time increment used, to develop numerical solutions for this regime. The time evolution of the atomic wave packet across the field is governed by the Schrödinger equation

$$i\hbar \frac{d\Psi}{dt} = (\mathscr{H}_{\rm kin} + \mathscr{V})\Psi, \tag{20}$$

wherein we have suppressed the time and position dependence of $\mathscr{H}_{\rm kin}$ and $\mathscr{V}$. For each time increment $\Delta t$, the atomic wave function, written as $\Phi(p,t)$ in momentum representation and $\Psi(z,t)$ in position representation, so that $\Phi(p,t) = \mathscr{F}\{\Psi(z,t)\}$, is evolved via

$$\Phi(t+\Delta t) = \exp(-iK\Delta t/2).\mathscr{F}\{\exp(-iV\Delta t) \times .\mathscr{F}^{-1}[\exp(-iK\Delta t/2)\Phi(p,t)]\}, \tag{21}$$

in which $K = \mathscr{H}_{\rm kin}/\hbar$ and $V = \mathscr{V}/\hbar$.

We have first investigated the idealized case of a monochromatic plane wave atomic beam interacting coherently with an optical field with a top hat profile. Since there is no slow turning on of the interaction, we cannot use adiabatic following to ensure the atom experiences the desired potential, so that we have prepared the atomic beam in the appropriate eigenstate. This is, of course, much easier to perform theoretically than in practice. The atomic distribution at the first focal plane is shown as the dash-dotted line in Fig. 8, using the same optical parameters as in the thin lens analysis, $\Omega = 2\sqrt{2}\Delta$. For this peak, $\mathscr{W}_c = 0.02\lambda_L$, with a FWHM of $0.016\lambda_L$. The interaction time $t_{\rm int} = 42.6|\Delta|^{-1}$ is determined empirically by finding the maximum value of the peak value of $|\psi(z,t)|^2$ as a function of interaction time with the field. This maximum value is plotted in Fig. 7 versus interaction time. It can be seen that the first focal plane gives the optimum focusing, subsequent focusings giving lower peaks. The predicted focal time for the parameters used, from the period as in Eq. (19), is $43.1|\Delta|^{-1}$, which differs from the empirically determined time by less than 2%. The atomic distribution at the predicted focus is almost indistinguishable from that at the actual focus.

We have also considered the more realistic case where the laser field is given a Gaussian profile, where it is not so easy to calculate the focal time except by inspecting the maximum of $|\psi|^2$ at each time increment. In an attempt to have the field exhibit a profile closer to the ideal top hat, we have added three Gaussian profile fields, spaced at one standard deviation apart. The standard deviation of each individual Gaussian, in the time frame which follows an individual atom, is $69/\sqrt{2}|\Delta|$, with the interaction being turned on at that point in the Gaussian where the effective Rabi frequency becomes $\Omega\exp(-9/2)$. This standard deviation is equivalent to the time for a sodium atom, at the rms velocity for a temperature of 1800 K, to travel 0.2 mm. At the center of the field, $\Omega = 2\sqrt{2}|\Delta|$. We have used the attributes of the sodium atom to set our length and mass scales, with the time scale set by having $\Delta = 200$ MHz. The 589 nm sodium wavelength, taken together with the unit values for $\hbar, k$, and $\Delta$, result in an atomic mass for the sodium atom of 634 in our particular system of units.

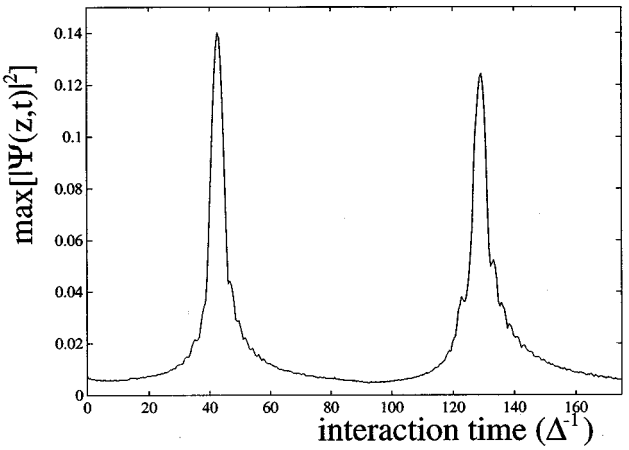


FIG. 7. Maximum of $|\psi(z,t)|^2$ as a function of flight time within the field, for the channeling system. In contrast to the thin lens system, we can see that the atoms will periodically focus and defocus, although the initial focus gives the best performance.

The results of our calculations are shown as the solid line in Fig. 8, which shows the atomic distribution at the first focal plane, after a flight time of $t_{\rm int} = 112.8|\Delta|^{-1}$. This is much longer than the flight time with a top hat profile because the atom experiences a much shallower potential in the

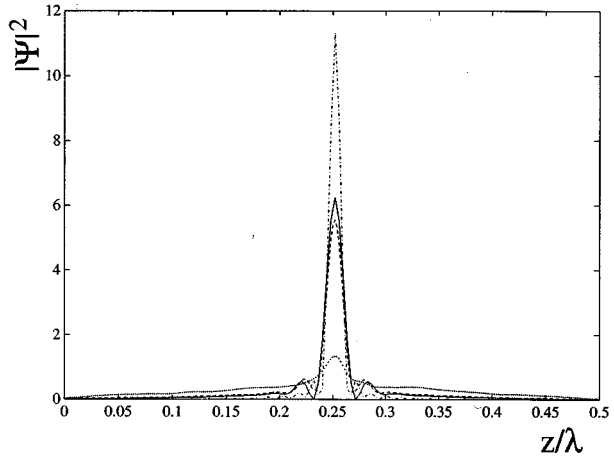


FIG. 8. The atomic distribution $|\psi(z,t_{\rm int})|^2$ after interaction time $t_{\rm int} = 42.6|\Delta|^{-1}$ within a field with a top hat profile is represented by the dash-dotted line. As the input atomic wave function was a plane wave, this distribution will repeat every $\lambda_L/2$. The second highest peak, with the solid line, represents the focused atomic distribution for channeling in a laser field with Gaussian profile and $t_{\rm int} = 112.8|\Delta|^{-1}$. The dashed line represents the distribution for the same parameters, but with spontaneous rates of $\gamma_1 = \gamma_2 = \Omega/100$. The lowest, dotted, line is for $\gamma_1 = \gamma_2 = \Omega/10$.

wings of the Gaussian. As in the thin lens case, the ladder atoms must enter the field in their ground state and a high degree of adiabatic following was present in our simulations. The focal peak is also more squat than for the top hat profile field, with $\mathscr{W}_c = 0.04\lambda_L$, although the FWHM measure has the same value. Comparison of the two atomic distributions in Fig. 8 shows that the FWHM measure is somewhat misleading.

## VI. BROADENING EFFECTS

The cases we have treated so far are simplified in both the quantum and classical senses. There will always be sources of quantum noise present, namely, spontaneous emission and laser amplitude and phase fluctuations. Spontaneous emission is often countered by tuning away from resonance, at the expense of weakening the interaction. However, the ratio $\Omega/\Delta$ must be preserved in order to obtain the required shape of potential. We must also consider completely classical broadening mechanisms. In classical optics the two main mechanisms affecting the performance of optical elements are chromatic and spherical aberration. Chromatic aberration, resulting from the different wavelengths present in light, has a counterpart in atom optics in that any input atomic beam will always have a three-dimensional velocity distribution. Spherical aberration results because optical lenses are usually ground using partly spherical surfaces rather than one of the Cartesian surfaces which give ideal performance. The counterpart in our schemes results from anharmonicity of the potential, in that it cannot be perfectly represented by a quadratic.

In practice, the effects of spontaneous emission can be minimized by increasing the field intensity, meaning that the interaction time is shortened, thus giving any individual atom less time in which to emit. Although the atoms used in experiments are usually sourced from an atomic oven, thereby possessing a Maxwellian velocity distribution, this can be adjusted by precooling and velocity selection mechanisms, thus minimizing the effects of differing interaction times. We have seen that the predictions of focal length using a quadratic approximation to the potential are very accurate, demonstrating that anharmonicity will not play a large role in these schemes. Although we have produced results in this paper for a particular ratio of Rabi frequency to detuning, our investigations show that this exact ratio is not as crucial as in the previously analyzed bichromatic beam splitter [15]. The potential remains closely harmonic over a reasonable range of values.

### A. Spontaneous emission

The extent to which spontaneous emission will degrade the performance of our systems will depend on several factors. Among these are the actual atoms used, the interaction time, and the laser intensity. Atoms which can be prepared in the ladder and $\Lambda$ configurations have an advantage in that they enter the interaction regime in a ground state and, hence must be Rabi cycled into an upper state before there is any possibility of emission. This does not hold for atoms in the $V$ configuration, for which the state which adiabatically follows the focusing potential is one of the excited states.

There are two ways in which spontaneous emission affects performance. The first is that the spontaneously emitted photon gives a momentum kick to the atom, meaning that it will no longer be exactly on a focusing trajectory. The second is that the internal state of the atom changes, so that it will no longer be in the eigenstate appropriate to the focusing potential. The relatively short times over which these mechanisms can take effect means that we would not expect the effects of spontaneous emission, all else being equal, to be as large as for the bichromatic beam splitter. In that application, we considered that all atoms were detected at infinity, in their ground state. This meant that, having left the field in an intermediate state, most experienced at least one emission on their way to the detector. The time involved meant that a small kick in momentum space could turn into a reasonable displacement in position space. In our present schemes, where the substrate is either within the field or a short distance beyond it, a small change in momentum will not have sufficient time to cause significant change in position.

Each spontaneous photon will give the emitting atom a momentum kick whose direction, and hence projection on the $z$ axis, will depend on the dipole distribution

$$\mathscr{N}(p') = \frac{3}{8\hbar k}\left[1+\left(\frac{p'}{\hbar k}\right)^2\right], \tag{22}$$

where $p' = \hbar k\cos\theta$, with $\theta$ the angle made by the photon direction and the $z$ axis [18]. In the thin lens, this process may also occur for atoms which leave the field in an excited state, since there is a possibility of decay en route to the substrate.

We have modeled these effects for ladder configuration atoms via the techniques of quantum Monte Carlo wave function simulation [19]. To perform this analysis for the thin lens, we add imaginary decay terms to the effective interaction Hamiltonian $\mathscr{V}$ so that it is no longer Hermitian,

$$\mathscr{V}_{\rm MC} = \frac{\hbar}{2}\begin{bmatrix} 0 & \Omega_1\sin kz & 0 \\ \Omega_1^*\sin kz & 2(\Delta_1 - i\gamma_1) & \Omega_2\sin(kz+\phi) \\ 0 & \Omega_2^*\sin(kz+\phi) & 2(\Delta_1+\Delta_2 - i\gamma_2) \end{bmatrix}. \tag{23}$$

In the above, $\gamma_1$ represents the spontaneous decay rate from $|2\rangle$ to $|1\rangle$, with $\gamma_2$ representing that from $|3\rangle$ to $|2\rangle$. Use of a non-Hermitian Hamiltonian to govern the time development of the wave function means that the norm of $\psi$ is now time dependent, decaying at a rate governed by the size of the spontaneous emission rates and the populations of the excited states. Comparison of the squared norm with randomly generated numbers between 0 and 1 is used to decide when a spontaneous emission takes place. Comparisons of the expectation values of the level populations with other random numbers are used to decide which level decays and the transverse component of the momentum kick is generated using random numbers in accordance with the distribution given above, Eq. (22). After each spontaneous emission, the wave function is renormalized and the process begins again, continuing until the atom has crossed the field. We then propagate the atom through space to the substrate, using $\mathscr{H}_{\rm kin}$ with decay terms added, and following a similar process to that used within the field. Summing a large number of

individual atomic trajectories and calculating the variance in the mean allows us to determine when the resulting atomic distribution will approach closely to that predicted by master equation techniques. We found that 200 trajectories were enough for the plus and minus one standard deviation plots to be almost indistinguishable from the mean on the scale we have used.

The result of a Monte Carlo calculation using decay rates of $\gamma_1=\gamma_2=\Omega/100$ [20] is reproduced as the solid line in Fig. 6. While there is a small amount of background present that does not exist in the coherent case and the height to width ratio is slightly reduced, the actual lensing performance is still acceptable. The 200 trajectories calculated experienced 115 spontaneous emissions within the field, with none between the field and the detector. The FWHM of this distribution is $0.020\lambda_L$, with $\mathscr{W}_c=0.053\lambda_L$. Our investigations show that the atomic distribution will not be significantly worse than the coherent case if the Rabi frequency can be raised to the order of 100 times the spontaneous emission rate.

On the other hand, we can see from the dash-dotted line in the same figure that, if the Rabi frequency is as low as ten times the spontaneous rate, the central focusing peak is still visible, but there is also a large amount of broad, flat background. With an average of 9.2 spontaneous emissions per trajectory, we now obtain a FWHM of $0.049\lambda_L$, with $\mathscr{W}=0.091\lambda_L$. Although these figures still suggest a reasonable focusing performance, they are in fact misleading. If, for example, we are interested in laying down narrow conduction paths on a resistive substrate, $|\psi|^2$ should go almost to zero over at least a reasonable portion of the half-wavelength width. In this case the broad background apparent in Fig. 6 would mean that electrons could be conducted everywhere across the substrate.

In the channeling scheme, spontaneous emission can only occur within the field. The main effect will be that an atom, after spontaneous emission, will no longer experience the focusing potential. Analysis of the situation proceeds almost as in the thin lens case, using the non-Hermitian Hamiltonian $\mathscr{V}_{MC}$ in a quantum Monte Carlo wave function simulation. As in the coherent case, we use the split-operator technique, also using the kinetic operator within the field. The result of a simulation of 200 trajectories with a spontaneous emission rate, $\gamma_1=\gamma_2=\Omega/100$, is shown as the dashed line in Fig. 8. The FWHM of this peak is $0.02\lambda_L$, with $\mathscr{W}_c=0.05\lambda_L$, resulting from 155 spontaneous emissions during an interaction time of $112.8\Delta^{-1}$. By comparing Fig. 6 with Fig. 8, we can see that, for a similar spontaneous rate, the effects on the two systems are very similar, as is to be expected. A larger spontaneous rate of $\Omega/10$, demonstrated by the dotted line in Fig. 8, has again degraded the performance considerably. For both systems, the field intensity will need to be such that the Rabi frequency is much greater than the spontaneous emission rate if we are to overcome the broadening effects of incoherent processes.

### B. Velocity distribution

In atom optics experiments involving atomic beams, the atoms are usually emitted from an oven operating at a relatively high temperature. The output of an oven at temperature $T$ will consist of atoms possessing a range of velocities which, to a close approximation, will obey a Maxwellian distribution with the probability of any atom having a velocity between $v$ and $v+dv$ being represented by

$$P(v)dv\propto v^3\exp(-mv^2/2kT), \tag{24}$$

where $m$ is the atomic mass, $k$ is Boltzmann's constant, and $T$ is the temperature in kelvins. The effect of this velocity distribution on the bichromatic atomic lens will be to cause the atoms to undergo the interaction for differing times and therefore become focused at different distances. In many atom optics experiments, the output of the oven is collimated, so as to give a small angular spread, and then put through an optical molasses setup which cools the beam in the transverse direction. As the longitudinal velocity will then be very much larger than any remaining transverse component, we feel justified in considering that the input to the field can be treated as having a zero transverse momentum component.

We have simulated a Maxwellian distribution for atoms with the sodium mass, emitted from an oven at 1800 K, by calculating individual trajectories with differing interaction times. The individual velocities are randomly chosen in accordance with the above distribution, Eq. (24). The focal length used is that for an atom at the rms velocity,

$$v_{\rm rms}=\sqrt{3kT/m}. \tag{25}$$

The extent to which this thermal velocity distribution degrades the focusing of the thin lens can be seen in Fig. 9, which is the result of 1000 trajectories in which spontaneous emission has been neglected. The input beam is considered as a plane wave and the laser field is given the same intensity profile as in Fig. 8. The FWHM for this distribution is $0.04\lambda_L$, with $\mathscr{W}_c=0.09\lambda_L$. It is immediately apparent that, to retain a good focusing performance, the spread in velocities will need to be narrowed by some means. We have considered that the beam can somehow be *chopped* so that only

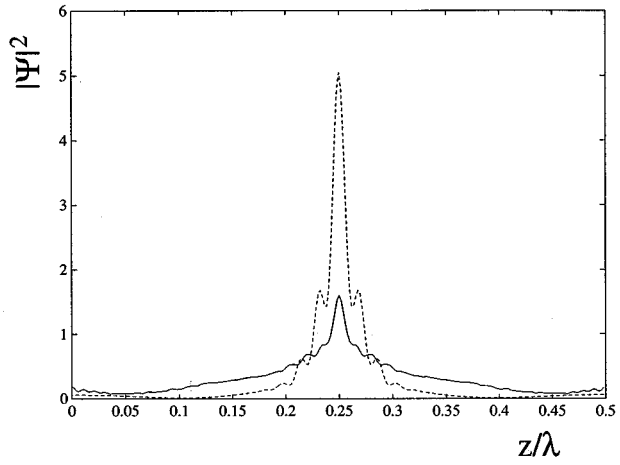


FIG. 9. Thin lens distributions for an atomic beam with the Maxwellian longitudinal velocity distribution considered. The solid line is the result for the full range of velocities, while the dashed line is for a Maxwellian longitudinal velocity distribution, somehow chopped so that only velocities from $0.9v_{\rm rms}$ to $1.1v_{\rm rms}$ remain.

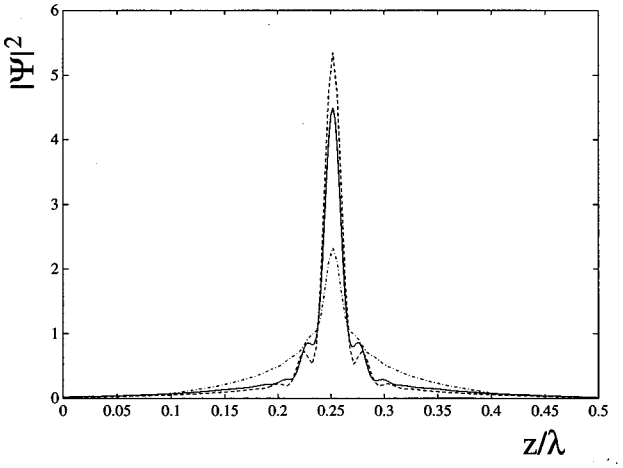


FIG. 10. Channeling distributions at the first focus for an atomic beam with Maxwellian longitudinal velocity distribution considered. The dash-dotted line includes velocities in the range $0.5v_{\rm rms}$–$1.5v_{\rm rms}$, while the solid and dashed lines include only those in the range $0.9v_{\rm rms}$–$1.1v_{\rm rms}$, with the dashed line representing coherent evolution and the solid line including the effects of spontaneous emission rates of $\gamma_1=\gamma_2=\Omega/100$.

a narrow spread of velocities about $v_{\rm rms}$ need be considered. The result for a distribution Maxwellian in form, but extending only over the range $v_{\rm rms}\pm 10\%$, is shown as the dashed line in Fig. 9. This distribution has a FWHM of $0.016\lambda_L$, with $\mathscr{W}_c=0.044\lambda_L$.

A longitudinal velocity distribution will affect the performance of the channeling system in exactly the same manner, as can be seen from Fig. 10. The dashed line represents a chopped distribution which includes velocities from $0.5v_{\rm rms}$ to $1.5v_{\rm rms}$, with FWHM of $0.023\lambda_L$ and $\mathscr{W}_c=0.06\lambda_L$. The solid line gives the results for a distribution from $0.9v_{\rm rms}$ to $1.1v_{\rm rms}$, with FWHM of $0.016\lambda_L$ and $\mathscr{W}_c=0.044\lambda_L$. Comparison of the peak shapes in Fig. 9 and Fig. 10 shows that the two numerical measures of the focusing performance are of limited utility, with more information available from the actual pictorial distributions.

In practice we can see that both systems will be relatively more sensitive to a distribution in atomic velocities than to spontaneous emission. This can be seen in the solid line of Fig. 10, which demonstrates the effects of both spontaneous emission, with $\gamma_1=\gamma_2=\Omega/100$, and a velocity range of $0.9v_{\rm rms}$–$1.1v_{\rm rms}$ on the channeling system. We can see that the resulting atomic distribution is closer to the dashed line of Fig. 10 than to the dashed line of Fig. 8, demonstrating that the velocity spread has had a greater effect than has spontaneous emission. The effects on the thin lens system are very similar.

We have seen that there are physical limits on the focusing performance of the two systems. The broadening mechanism which can be expected to have the most marked effect is the range of longitudinal velocities in the input atomic beam, the analog of chromatic aberration in classical optics. Although this velocity distribution is a completely classical phenomenon, the extent to which the input beam can be cooled will ultimately depend on quantum limits. Defocusing due to anharmonicity of the potential can be minimized by careful choice of atomic transitions, while the effects of spontaneous emission can be ameliorated by choice of atom and an increase of laser power. One broadening effect we have not considered, which is mentioned by McClelland *et al.* [12], is possible movement of atoms on the substrate after deposition.

## VII. CLASSICAL TREATMENT OF CHANNELING

The channeling of atoms in a harmonic optical potential has a classical analog in the motion of point masses in a parabolic well. It is well known that the time for particles to reach the bottom of a parabolic well is independent of initial position, resulting in the particles all reaching the bottom at the same time. This time can be calculated exactly as in the optical channeling treated above, Eq. (19).

It is of interest to investigate a classical treatment of channeling for two reasons. First, comparison with the quantum results obtained above will demonstrate if there are any distinctly quantum features of the interaction. Secondly, on a more practical level, the classical calculations are less expensive in terms of computation time. If an experimenter, for example, wishes to investigate the change in focal length as parameters are varied, it is much quicker to run a classical simulation than a full quantum one.

The extent to which purely quantum effects exist is best found by investigating the simplest scenario, in which we consider the motion of evenly spaced point masses, analogous to a plane wave, in the potential obtained by diagonalization of the interaction Hamiltonian, Eq. (7). The transverse force on each mass is found by differentiation of the potential, and Newton's laws then give the resulting velocity and position. In this simplest case, we consider that the potential and the longitudinal velocity of the point masses both remain constant. The masses initially have zero transverse momentum. We found that the best focusing performance occurred after a time which was the average for the masses to reach the center of the potential. As in the quantum case, this time was very close to that calculated using a quadratic approximation for the potential. The result of this basic calculation, analyzing the trajectories of 1000 point masses, shows that the classical distribution is narrower than the quantum one. There is a classically forbidden region, in which no particles are present, whereas in the quantum analysis there is a small, but nonvanishing probability that an atom will be found in this region.

We have also investigated the more realistic situation in which the potential is not constant, but has the same profile as the Gaussian laser field, and the point masses have a thermal longitudinal velocity distribution. The potential is that which an atom would experience with perfect adiabatic following. We have considered the effects of coherent evolution only since, although the random momentum kicks of spontaneous emission could be simulated classically, the different potential experienced by an atom which has emitted is not so easily simulated. As our motivation is to develop a simpler method of predicting the broad features of the atomic motion, and, as shown above, the velocity distribution is the main contributor to broadening of the focused distribution, we have ignored spontaneous emission.

The results of a classical analysis with parameters which are the equivalent of those used for the dashed line of Fig. 8

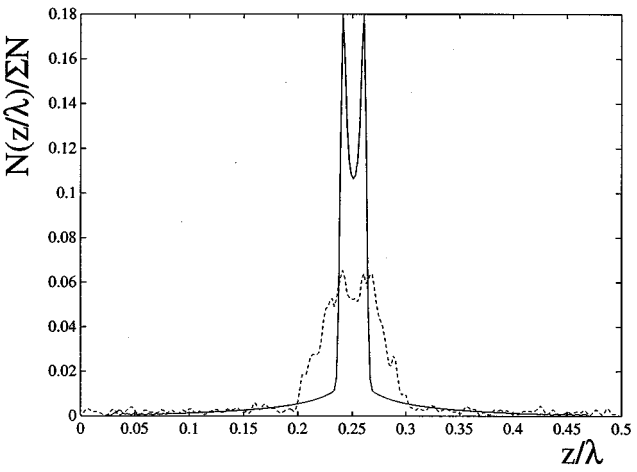


FIG. 11. The results of classical calculations for the focusing of 1000 equally spaced point masses in the quantum potential. The masses have zero initial transverse momentum. The solid line is the result when all masses have the same longitudinal velocity. The dashed line represents masses with an initial longitudinal velocity distribution extending from $0.9v_{\rm rms}$ to $1.1v_{\rm rms}$.

are shown as the solid line in Fig. 11. All point masses are considered to have the same longitudinal velocity and the potential has a Gaussian longitudinal profile. While the shapes of the two distributions are different, with the classical result showing a double peaked structure and having greater width, the focal lengths are almost exactly the same, despite being found by different methods. This shows that a relatively simple classical computation of channeling could be of practical use in finding the optimum position for the substrate, even though, as discovered by McClelland *et al.* [12] it will not accurately predict the profile of the atomic distribution. The dashed line in Fig. 11 is the classical result for a chopped Maxwellian distribution, including $0.9v_{\rm rms}-0.9v_{\rm rms}$, and a Gaussian profile field. Comparison with the dashed line in Fig. 10 shows that the classical and quantum results are only qualitatively similar, although the focal length is again accurately predicted. This provides evidence that the fine features of the resulting atomic distribution result from the quantum effects of interference within the wave function, rather than from any classical effects.

## VIII. TWO-LEVEL COMPARISON

Some of the practical difficulties involved in the bichromatic atomic lens, such as finding atoms possessing transitions which can take the required form and tuning two separate standing waves, mean that it would not be worth persevering with unless it offers clear advantages over a two-level system. The obvious advantage is that the bichromatic potential is much closer to being harmonic over its full width, whereas the potential from a single standing wave is approximately harmonic for only a fraction of the width. This will mean that much narrower focusing is possible with the bichromatic lens, without having to prepare the width of the input atomic beam. The chromatic aberration resulting from different atomic velocities will have more of an effect on the two-level system, as fast atoms beginning in the wings of the potential will experience a smaller phase shift, hence less deviation towards the center than in the bichromatic lens. This will result in a broadening of the focused distribution. Spontaneous emission will not be expected to have any greater effect in the bichromatic lens if ladder or $\Lambda$ configuration atoms are used, as it is a ground state which adiabatically becomes the eigenstate of the focusing potential.

We have performed numerical simulations using two-level atoms for both the thin lens and channeling systems. The degree of harmonicity of the two-level potential depends on the ratio $\Omega/\Delta$, with an increasing ratio giving a better coherent focusing performance. Unfortunately this is also the regime where spontaneous emission begins to have a marked effect. Our investigations show that the bichromatic lens produces an atomic distribution which has a height to width ratio which is at least 1.7 times greater than can be expected from a two-level lens. We find that there is more broad background around the central peak in the two-level case and our measure of width, $\mathscr{W}_c$, is at least 50% greater with the monochromatic lens, all else being equal. These results demonstrate that the bichromatic lens has clear advantages in performance over an atomic lens using a single standing wave and two-level atoms.

## IX. CONCLUSION

We have investigated the performance of a proposed atomic lens using three-level atoms and two standing wave optical fields. The focusing potential can in principle be made very close to the ideal harmonic shape and the focal lengths for both the thin lens and channeling systems can be accurately predicted. We have shown that spontaneous emission will not play a major role in performance degradation if the laser intensities are high enough. The main cause of broadening will be the differing velocities present in an atomic beam. Some effort will need to be made to prepare the input beam to have as small a range of velocities as possible. We have shown that the bichromatic lens, because of the near harmonicity of the potential, offers clear advantages over atomic lenses using two-level atoms.

There is an experimental freedom in the choice of atomic configuration since spontaneous emission does not play a major role. The important factors in the choice of atom will be the optical wavelength of the transition and the lifetime of the lowest of the three levels used. The shorter the wavelength, the better the available focusing will be. The lowest level lifetime will need to be long enough that, once pumped into the appropriate starting level, most of the atoms will not emit from this level before deposition on the substrate has occurred. There seem to be many possible choices for $\Lambda$ and $V$ systems, with, for example, the alkali-metal atoms as used in velocity selective coherent population trapping having suitable transitions. Atoms having ladder transitions with suitable energies are more difficult to find. One possible candidate is rubidium as used by Grove *et al.* [11]. The adjacent transitions have wavelengths of 780.2 nm and 776.0 nm, so that $k_2 \approx 1.005 k_1$, meaning that the potential is close to the optimum over a region approximately 20 wavelengths in width.

It will be possible to deposit very narrow lines of atoms, with widths of very much less than the wavelength of the

optical transitions used, if the input beam can be prepared appropriately. The background present between these lines is small enough that this technique could have possible applications in, for example, the fabrication of circuitry components. It should also be possible to deposit very small *dots* of atoms by using two orthogonal bichromatic lenses, either sequentially or simultaneously.

## ACKNOWLEDGMENTS

This research was supported by the New Zealand Foundation for Research, Science and Technology and the University of Auckland Research Council. The authors also wish to thank Craig Blockley for useful discussions.

[1] C. Adams, M. Sigel, and J. Mlynek, Phys. Rep. **240**, 143 (1994).
[2] D. F. Walls and G. J. Milburn, *Quantum Optics* (Springer-Verlag, Berlin, 1994). Chapter 17 gives an overview of atomic optics.
[3] P. L. Kapitza and P. A. M. Dirac, Proc. Cambridge Philos. Soc. **29**, 297 (1933).
[4] S. Altshuler, L. M. Frantz, and R. Braunstein, Phys. Rev. Lett. **17**, 231 (1966).
[5] P. L. Gould, G. A. Ruff, and D. E. Pritchard, Phys. Rev. Lett. **56**, 827 (1986).
[6] V. S. Letokhov, Pis'ma Zh. Éksp. Teor. Fiz. **7**, 348 (1968) [JETP Lett. **7**, 272 (1968)].
[7] A. P. Kazantsev, G. A. Ryabenko, G. I. Surdutovich, and V. P. Yakovlev, Phys. Rep. **129**, 75 (1985).
[8] C. Salomon, J. Dalibard, A. Aspect, H. Metcalf, and C. Cohen-Tannoudji, Phys. Rev. Lett. **59**, 1659 (1987).
[9] M. G. Prentiss, N. P. Bigelow, M. S. Shahriar, and P. R. Hemmer, Opt. Lett. **16**, 1695 (1991).
[10] U. Janicke and M. Wilkens, J. Phys. (France) II **4**, 1975 (1994).
[11] T. T. Grove, B. C. Duncan, V. Sanchez-Villicana, and P. L. Gould, Phys. Rev. A **51**, R4325 (1995).
[12] J. J. McClelland, R. E. Scholten, E. C. Palm, and R. J. Celotta, Science **262**, 877 (1993).
[13] R. Gupta, J. J. McClelland, Z. J. Jabbour, and R. J. Celotta, Appl. Phys. Lett. **67**, 1378 (1995).
[14] Craig Blockley (private communication).
[15] T. Wong, M. K. Olsen, S. M. Tan, and D. F. Walls, Phys. Rev. A **52**, 2161 (1995).
[16] U. Janicke and M. Wilkens, Phys. Rev. A **50**, 3265 (1994).
[17] J. A. Fleck, Jr., J. R. Morris, and M. D. Feit, Appl. Phys. **10**, 129 (1976).
[18] Y. Castin, H. Wallis, and J. Dalibard, J. Opt. Soc. Am. B **6**, 11 (1994).
[19] *An Open Systems Approach to Quantum Optics*, edited by H. Carmichael, Lecture Notes in Physics Vol. m18 (Springer-Verlag, Berlin, 1993).
[20] It should be noted that, while we have used certain attributes of the sodium atom in our simulations, we have used totally arbitrary spontaneous emission rates, simply for the purposes of comparison.